Daytime ionospheric *D* region sharpness derived from VLF radio atmospherics

Feng Han,[1] Steven A. Cummer,[1] Jingbo Li,[1] and Gaopeng Lu[1]

Received 17 November 2010; revised 17 February 2011; accepted 3 March 2011; published 17 May 2011.

[1] We described and applied a technique to measure the local midlatitude daytime ionospheric *D* region electron density profile sharpness from the Earth-ionosphere waveguide mode interference pattern in the spectra of radio atmospherics (or sferics for short), which are the high-power, broadband, very low frequency (VLF, 3–30 kHz) signals launched by lightning discharges. VLF propagation simulations are used to show that the upper VLF frequency spectral minima of sferics on several hundred kilometers long propagation paths depend critically on the effective *D* region sharpness while depending only weakly on the effective *D* region height. This enables the straightforward extraction of the sharpness parameter from measured VLF spectra, which generally exhibit well-defined minima at upper VLF frequencies. By applying this technique, we calculated the profile sharpness during morning, noontime, and afternoon periods in 3 different days using sferics from ~660–800 km away. The measured sharpness showed a weak dependence on the solar zenith angle, with values between 0.35 and 0.45 km^{-1} for angles from 20° to 75°. This is different from the previous narrowband measurement since the sharpness derived from narrowband VLF signals highly depends on the solar zenith angle. To better understand this discrepancy, we also used simulations to calculate the equivalent exponential profiles for International Reference Ionosphere (IRI) profiles and the empirical FIRI model profiles. The equivalent exponential profiles can best duplicate the sferic spectral characteristics for IRI and FIRI models. We find that both the magnitudes and solar zenith angle variations of the sharpness for our broadband measurements, previous narrowband measurements, and both models are completely different. This suggests the daytime ionosphere, particularly at larger solar zenith angles, may not be well described by a simple two-parameter exponential model.

Citation: Han, F., S. A. Cummer, J. Li, and G. Lu (2011), Daytime ionospheric *D* region sharpness derived from VLF radio atmospherics, *J. Geophys. Res.*, *116*, A05314, doi:10.1029/2010JA016299.

1. Introduction

[2] Very low frequency (VLF, 3–30 kHz) and low-frequency (LF, 30–300 kHz) signals are a powerful tool for probing the ionospheric *D* region electron density. Previous work along these lines has mainly focused on measurements using single frequency or narrowband signals transmitted by large man-made transmitters and reflected by the lower ionosphere. Modern applications of this technique have measured amplitudes and phases for narrowband VLF signals sent by different transmitters and propagating long distances in the Earth-ionosphere waveguide, and compared the measurements to Long Wave Propagation Capability (LWPC) [*Pappert and Ferguson*, 1986] simulations, so as to infer the average *D* region electron density profiles along the wave propagation paths [*Thomson*, 1993; *Thomson and Clilverd*, 2001; *Thomson et al.*, 2004, 2005, 2007; *Thomson and McRae*, 2009; *Thomson*, 2010; *McRae and Thomson*, 2000, 2004].

[3] The broadband VLF sferic signals radiated by lightning strokes and reflected several times in the Earth-ionosphere waveguide can also be used to remote sense the ionospheric *D* region electron density profile variations. By using the waveform of a sferic in time domain, researchers derived the *D* region reflection height of radio waves from the arrival time difference between the ground wave and sky waves. *Smith et al.* [2004] calculated the *D* region virtual height as a function of local time (LT) from VLF/LF electric fields radiated by intracloud lightning and recorded by the Los Alamos Sferic Array (LASA). *Jacobson et al.* [2007] retrieved the *D* region reflection heights by using LF range Narrow Bipolar Events (NBE) sferic waveforms, and studied the virtual height variations with time, geographical locations and solar radiation.

[4] Broadband VLF sferic spectra were also used to infer the *D* region electron density profiles by fitting the measured spectra to modeled spectra. This approach was first suggested by *Cummer et al.* [1998]. In this technique (as in the narrowband technique of Thomson and coworkers),

[1]Department of Electrical and Computer Engineering, Duke University, Durham, North Carolina, USA.

0148-0227/11/2010JA016299

the D region electron density is modeled by a two-parameter exponential profile [*Wait and Spies*, 1964]. The height parameter controls the overall altitude of the profile while the sharpness represents the gradient of the electron density and is closely related to the inverse scale height. The spectra of measured sferics excited by several lightning strokes in different geographical locations were compared against LWPC modeled spectra, and the least squares error fitting was applied to find the best fitted two parameters, i.e., the D region electron density profiles. This work was later extended to D region variations of 16 nights and their correlation with energetic electron precipitation by *Cheng et al.* [2006]. *Cheng and Cummer* [2005] also used the similar method to quantitatively analyze the D region disturbance caused by three possible different mechanisms including electromagnetic pulses (EMPs), quasi-electrostatic (QE) fields and lightning-induced electron precipitation (LEP). An alternative method used to derive the D region electron density profiles from broadband LF sferics was recently proposed by *Jacobson et al.* [2009, 2010]. They sought the best D region electron density parameters via comparisons of measured data with a full-wave reflection numeric model outputs.

[5] More systematic measurements of the D region electron density were given by *Han and Cummer* [2010a, 2010b]. The D region equivalent exponential electron density profile height variations over 2 months were measured by fitting a series of finite difference time domain (FDTD) model [*Hu and Cummer*, 2006] simulated sferic spectra to the measured spectra from more than 350,000 sferics. The nighttime profiles were derived from the spectrum fitting in the frequency range 3–8 kHz whereas the daytime in 1.5–4 kHz. Each lightning stroke was treated as an independent transmitter and the average electron density profile height across the wave propagation path was calculated. Statistical results of measured temporal and spatial height variations were derived for the nighttime D region [*Han and Cummer*, 2010a]. The nighttime height varied widely and the average height in 2 months was consistent with the previous narrowband measurement [*Thomson et al.*, 2007]. Quantitative relations between the electron density height changes and solar zenith angles as well as solar flare X-ray fluxes were derived for the daytime D region [*Han and Cummer*, 2010b]. Both the height variations with the solar zenith angle and with the solar flare X-ray fluxes were consistent with the narrowband measurements given by *McRae and Thomson* [2000].

[6] However, in both nighttime and daytime measurements by *Han and Cummer* [2010a, 2010b], the D region electron density profile sharpness was not measured and was assumed as a constant. *Cummer et al.* [1998] suggested a method for measuring based on the interference amplitude, but our attempts to apply it to many signals indicated that it does not work reliably. In this work, we described and applied a different technique for measuring the profile sharpness independent of the height, which is based on the frequency of spectral minima from waveguide mode interference at upper VLF frequencies (~20 kHz). FDTD model simulations of broadband VLF propagation were used to show that the frequencies of these minima are strongly dependent on sharpness in a way that the lower-frequency spectral variations used to measure profile height [*Han and Cummer*, 2010a, 2010b] are not.

[7] To demonstrate the technique, we extracted the mid-latitude daytime D region electron density profile sharpness variations across solar zenith angles from 20° to 75° in 3 different days from measured average broadband VLF spectra. The resulting sharpness variations show weak dependence on solar zenith angles, which is somewhat different from what have been previously reported based on narrowband VLF propagation measurements on much longer propagation paths. We also derived the equivalent exponential profiles for International Reference Ionosphere (IRI) profiles and a semiempirical model from rocket-based measurements, called FIRI empirical model [*Friedrich and Torkar*, 2001], and found that both the magnitudes and solar zenith angle variations of the sharpness for broadband measurements, narrowband measurements, IRI and FIRI models are significantly different.

2. Sferic Data and Propagation Modeling

2.1. Description of Experimental Data

[8] National Lightning Detection Network (NLDN) provides the lightning timing and geolocation [*Cummins et al.*, 1998] that enable us to identify the source locations of the measured sferics. The sferic data are recorded by broadband VLF/ELF receivers located near Duke University [*Li et al.*, 2008]. Although both azimuthal (B_ϕ) and radial (B_r) components of the horizontal magnetic fields can be calculated from the two measured orthogonal signals, we only use B_ϕ [*Cummer et al.*, 1998; *Cheng et al.*, 2006; *Han and Cummer*, 2010a, 2010b] in order to avoid low signal-to-noise ratio (SNR), and thus increase the reliability of the measured results. Sferic data in July and August 2005 were used because the data acquisition system worked in continuous mode in these 2 months, and a favorable number of sferics in a small geographical region and short time window can be used to calculate the average spectrum.

2.2. Model Simulations of VLF Sferic Propagation

[9] The D region electron density profiles are derived by comparing the measured sferic spectra to the FDTD simulation results. In FDTD simulations, we use the standard D region electron density profile parameterizations of

$$N_e(h) = 1.43 \times 10^7 \exp(-0.15h') \times \exp\left[(\beta - 0.15)\left(h - h'\right)\right] \text{ cm}^{-3} \quad (1)$$

with h' in km and β in km^{-1} [*Wait and Spies*, 1964]. This functional form has been successfully used in VLF measurements [*Cummer et al.*, 1998; *McRae and Thomson*, 2000; *Cheng et al.*, 2006; *Thomson et al.*, 2007; *Thomson and McRae*, 2009; *Han and Cummer*, 2010a, 2010b]. The parameter h' controls the height of the electron density profile while β controls the sharpness of the profile. Continuous h' measurements have been reported by *Han and Cummer* [2010a, 2010b], and the objective of this work is to derive β from the sferic spectrum in higher-frequency range. The classic ion density profiles [*Narcisi*, 1971] are used and their feasibility was validated by *Cummer et al.* [1998] and *Han and Cummer* [2010a, 2010b]. We performed FDTD model

simulations and found that an increase in the ion densities by a factor of 10 has a negligible effect on waveguide mode interference patterns from which the equivalent exponential electron density profile is extracted. In order to compare our measured β to the results given by *McRae and Thomson* [2000], we use the collision frequency profiles [*Wait and Spies*, 1964; *Morfitt and Shellman*, 1976] which are widely used in VLF literature [*Cummer et al.*, 1998; *McRae and Thomson*, 2000; *Thomson et al.*, 2007; *Han and Cummer*, 2010a, 2010b]. There are other measured *D* region collision frequency profiles [*Phelps and Pack*, 1959; *Thrane and Piggott*, 1966; *Friedrich and Torkar*, 1983]. We performed FDTD model simulations and found that a change from the profile adapted from *Thrane and Piggott* [1966] to the profile from *Wait and Spies* [1964], around an increase in the frequencies by a factor of 3, can shift the sferic spectrum, which is equal to a shift caused by 0.07 km^{-1} β change. It means an uncertainty of 0.07 km^{-1} in β measurement is caused by an uncertainty of 3 times of the collision frequency.

[10] Because the simulated sferic wave propagation is in the midlatitude and the size of simulation domain (propagation distance ~700–800 km) is much smaller than Earth radius, the vector geomagnetic field is treated as homogenous in the whole simulation domain in all the simulations with the magnitude 5×10^4 nT and dip angle 65°, which are the values near Duke University. The azimuth dependence of the wave propagation is also included by ensuring that the propagation direction relative to the horizontal component of the background magnetic field reflects the real propagation geometry [*Hu and Cummer*, 2006].

[11] The upper boundary of the simulation domain is modeled by the two-parameter electron density profile described by (1). The physical parameters of the lower boundary depend on the sferic propagation paths. If the sferic propagation path is over the ocean, the lower boundary can be treated as a Perfect Electrical Conductor (PEC) since the seawater conductivity is large enough. FDTD model simulations showed that sferic spectra at frequencies less than 30 kHz are almost identical for the PEC boundary and Surface Impedance Boundary Conditions (SIBC) [*Maloney*, 1992; *Kellali and Jecko*, 1993] with the typical seawater conductivity 4 S/m [*Balanis*, 1989]. However, if the sferic propagation path is in the land, the small ground conductivity 0.004 S/m near Duke University (referenced to the ground conductivity map given by the Federal Communications Commission (http://www.fcc.gov/mb/audio/m3/index.html) and *Fine* [1954]) must be taken into account, and only SIBC can be used for the ground boundary. Note this 0.004 S/m ground conductivity is for AM broadcast frequencies, and the penetration depth is less than at VLF. Therefore, for a sferic wave from south, west and northeast, (azimuth angle from 180° to 360° and 0 to 45°), the whole propagation path is in the land and SIBC are used for all the FDTD model simulations. For a sferic wave from northeast to south (azimuth range from 45° to 180°), since more than half of the wave propagation path is over the ocean, we use the PEC ground boundary condition.

[12] The FDTD model does not support partial ground and partial seawater boundary condition. The PEC approximation of the partial sea and partial soil leads to an error in the β measurement. FDTD model simulations showed that a change from all sea (treated as a PEC) to all soil with conductivity 0.004 S/m in a 720 km propagation path caused an increase of 0.05 km^{-1} in the β measurement. If we consider a smaller ground conductivity $\sigma = 0.001$ S/m which has been used by *Thomson* [2010], this increase is 0.08 km^{-1}. However, in all our measurements for azimuth angle in 45°–180° range, the real sferic wave propagation paths have more than half in the seawater, and therefore the β measurement error caused by the PEC approximation is less than 0.04 km^{-1} for ground conductivity $\sigma = 0.001$ S/m, whereas less than 0.03 km^{-1} for ground conductivity $\sigma = 0.004$ S/m, if we assume the linear change of the error with distance. This means the measured β values in this work using PEC approximation for the partial sea and partial ground are smaller than the true values by less than 0.03–0.04 km^{-1}. For the sferic in an all land path (azimuth angle from 180° to 360° and 0 to 45°), the measured β is 0.03 km^{-1} smaller if we use the ground conductivity $\sigma = 0.004$ S/m instead of 0.001 S/m.

[13] In addition, Perfect Matched Layers (PML) were used to absorb outward propagating sferic waves so as to avoid artificial reflections [*Hu and Cummer*, 2006]. The source lightning return stroke in FDTD simulations was modeled by *Jones* [1970] and *Dennis and Pierce* [1967] which was used by *Cheng et al.* [2006] and *Han and Cummer* [2010a, 2010b], and had no effect on the results because β values were derived from Earth-ionosphere waveguide mode interference patterns.

3. The Influence of β on VLF Sferic Higher-Frequency Band

[14] The daytime *D* region electron density profile parameter h' can be derived from the sferic spectrum in the frequency range 1.5–4 kHz [*Han and Cummer*, 2010b] because larger h' can shift the Earth-ionosphere waveguide mode interference patterns to lower-frequency ranges. FDTD model simulations in that work showed that the mode interference pattern (the peaks and valleys) in this frequency range is not sensitive to changes in β. In contrast, we show here that spectral minima are sensitive to β values at higher-frequency range (~15–25 kHz, varying somewhat as the ionosphere or lightning distance changes). This sensitivity forms the base of β derivation from VLF sferic spectra.

[15] Figure 1 shows the effects of β on the mode interference pattern of sferic spectra in different frequency ranges. In all these simulations, we chose distances = 500 km and azimuth angles = 90° as representatives. Figure 1a shows five sample exponential daytime electron density profiles and Figure 1b shows the corresponding simulated sferic spectra across the full VLF bandwidth. Figures 1c and 1d show the detailed spectra in lower-frequency range and higher-frequency range. For the same h' value but different β values, the valley positions of mode interference patterns in the lower-frequency range are essentially the same [*Han and Cummer*, 2010b]. However, the spectral minimum in the higher–VLF frequency range clearly shifts down as β increases, as shown in Figure 1d. It is from the position of this minimum that the β is derived. Although the amplitudes of peaks and valleys are also affected by β, they cannot be directly used to derive β because they are rather variable in the measured sferic spectra, which is probably caused by

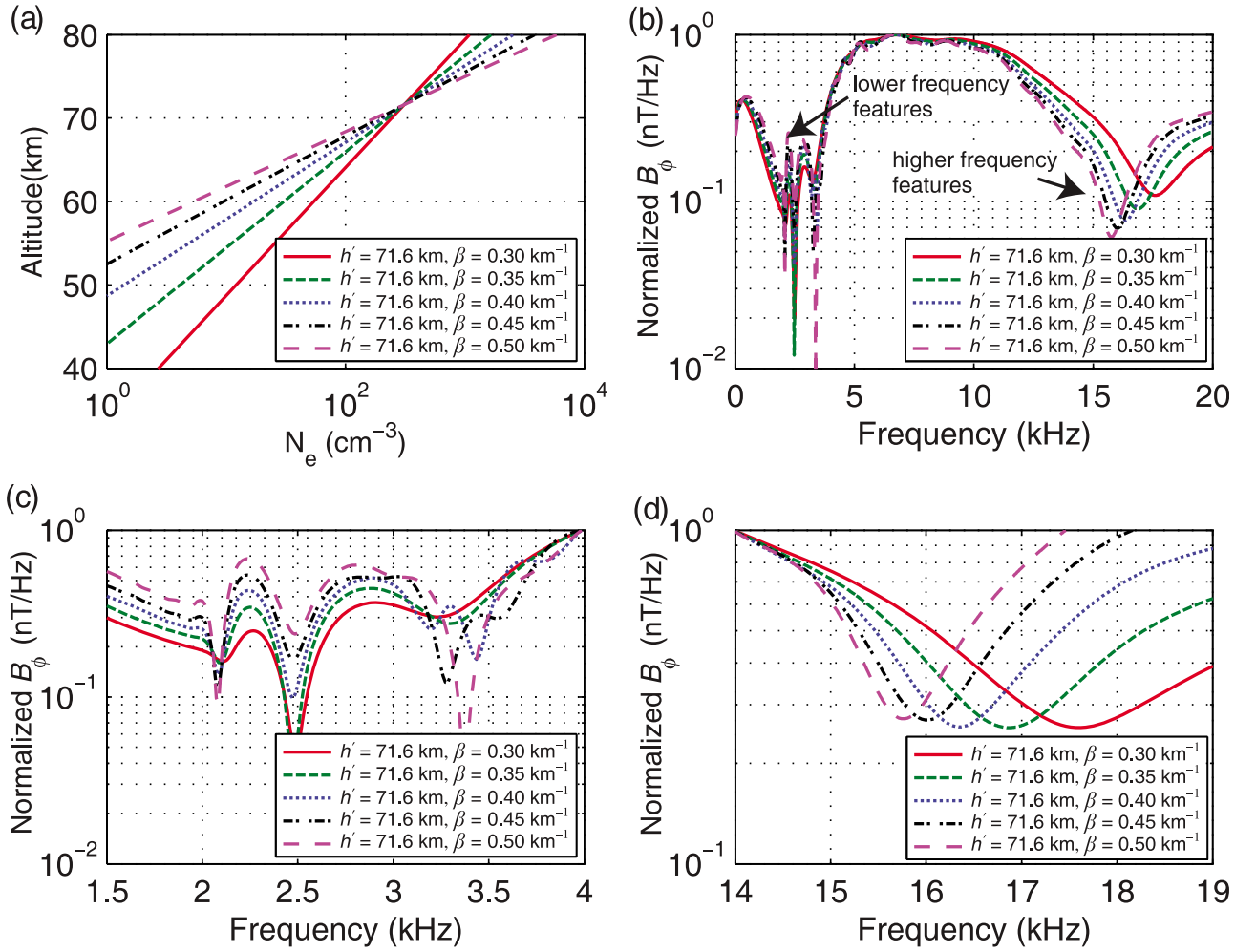

Figure 1. Five typical daytime *D* region electron density profiles and corresponding simulated sferic spectra under these profiles: (a) electron density profiles, (b) the general shapes of sferic spectra normalized by the maximum amplitudes in the 5–10 kHz range, (c) the lower-frequency sferic spectra normalized by amplitudes in 4 kHz, and (d) the higher-frequency sferic spectra normalized by amplitudes in 14 kHz. The mode interference patterns in the lower-frequency range are not sensitive to β, but those in the higher-frequency range are obviously sensitive to β.

complicated source lightning waveforms and different channel orientations.

[16] Additional simulations for daytime ionospheres show that this upper VLF minimum is sensitive to propagation distances but only weakly dependent on propagation azimuth angle; that is, a larger distance shifts the fine frequency structures up in frequency, whereas a change of 30° of the azimuth angle has little effect on them. This requires the precise values of propagation distance but less precise values of propagation azimuth in all FDTD simulations.

4. Measured Daytime β

[17] To give an overview of typical daytime β variations, we computed β in three periods: morning, noontime and afternoon. We selected these three periods in 3 different days (19 July, 12 August, and 6 August, 2005) for following reasons. In these days, there were sufficient sferics (from 20 to 69) in 5 min time windows originating from small geographical regions. Each period lasted more than 3 h. In each period, in every ~30 min, we chose a 5 min time window that is long enough to include several tens of lightning strokes but short enough so that the large-scale *D* region electron density is not likely to change significantly [*Cummer et al.*, 1998; *Cheng et al.*, 2006]. In each 5 min time window, several tens of lightning strokes from a small geographical region (~20 km × 20 km) were selected. These lightning strokes were located in almost the same geographical region, and thus the sferic spectra excited by them almost had the same features.

[18] In each 5 min window, we calculated the average sferic spectrum excited by these lightning strokes in order to lower the noise level in the measured sferic spectra [*Cummer et al.*, 1998]. Figure 2 shows two examples of the extraction of h' and β. Figures 2a and 2b show the electron density profile measurement at 0938 LT on 19 July 2005. The measured sferic spectrum is the average of 53 spectra generated by lightning strokes approximately 754 km from

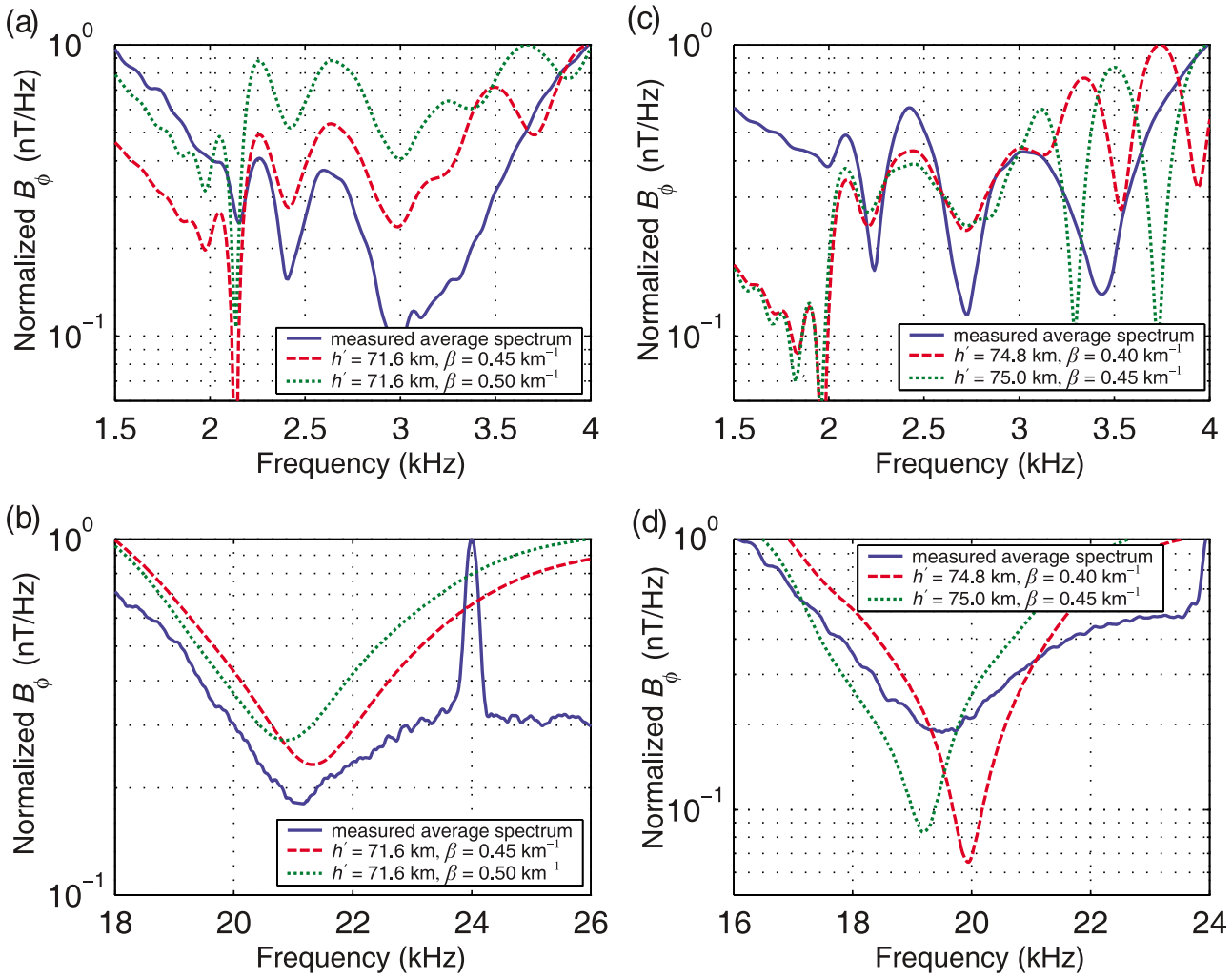

Figure 2. The procedure for the electron density profile measurements from sferic spectra fitting shown by two examples: (a) h' derived from the lower-frequency mode interference pattern at 0938 LT, (b) β derived from the higher-frequency mode interference pattern at 0938 LT, (c) h' derived from the lower-frequency mode interference pattern at 0738 LT, and (d) β derived from the higher-frequency mode interference pattern at 0738 LT on 19 July 2005.

Duke sensors and located in the east direction (azimuth angle ~90°). Figure 2a shows the best fitted h' = 71.6 km retrieved from alignments of those valleys of the mode interference pattern in the lower-frequency range, as discussed by *Han and Cummer* [2010b]. However, the spectrum in this frequency range is not sensitive to β and gives equally good fits for β = 0.45 and 0.50 km^{-1}. In contrast, the frequency of the mode interference minimum in the simulated spectrum near 20 kHz is very sensitive to β. The best fit to the measured spectrum is located between the simulated spectra for β = 0.45 and 0.50 km^{-1}. By using linear interpolation, we found the best fitted β = 0.47 km^{-1}. Figures 2c and 2d show the profile measurement in the same day but at 0738 LT. The best fitted h' is 74.9 km and the best fitted β is 0.42 km^{-1}. As shown in Figure 2c, the measured and simulated minima and maxima above 3.5 kHz are not well aligned. This is caused by the difference between the complex real *D* region electron density profile and the exponential profile we used in the FDTD model simulations. The h' measurement mainly depends on the middle valley alignment (near 2.7 kHz in this example) in the lower-frequency range [*Han and Cummer*, 2010b]. Sometimes, the spectra valleys in both the lower- and higher-frequency ranges are not precisely aligned, and this leads to an error in β measurement. By using the measurement at 0738 LT on 19 July 2005 which is shown in Figures 2c and 2d, we first estimate the error caused by the uncertainty of the measured sferic spectrum valley position in the "relative flat" higher-frequency range 19.33–19.75 kHz. The β measurement error caused by such a valley position uncertainty is ±0.014 km^{-1}. In addition, we found, in the lower-frequency range, the valley positions of the simulated spectra for h' ±0.2 km deviation from best fitted h' value and those of measured spectrum are obvious different. This less than ±0.2 km h' uncertainty leads to the sferic spectrum valley position uncertainty in the higher-frequency range. We estimated the β measurement error caused by this ±0.2 km h' uncertainty and found it is ±0.009 km^{-1}. Therefore, the total β mea-

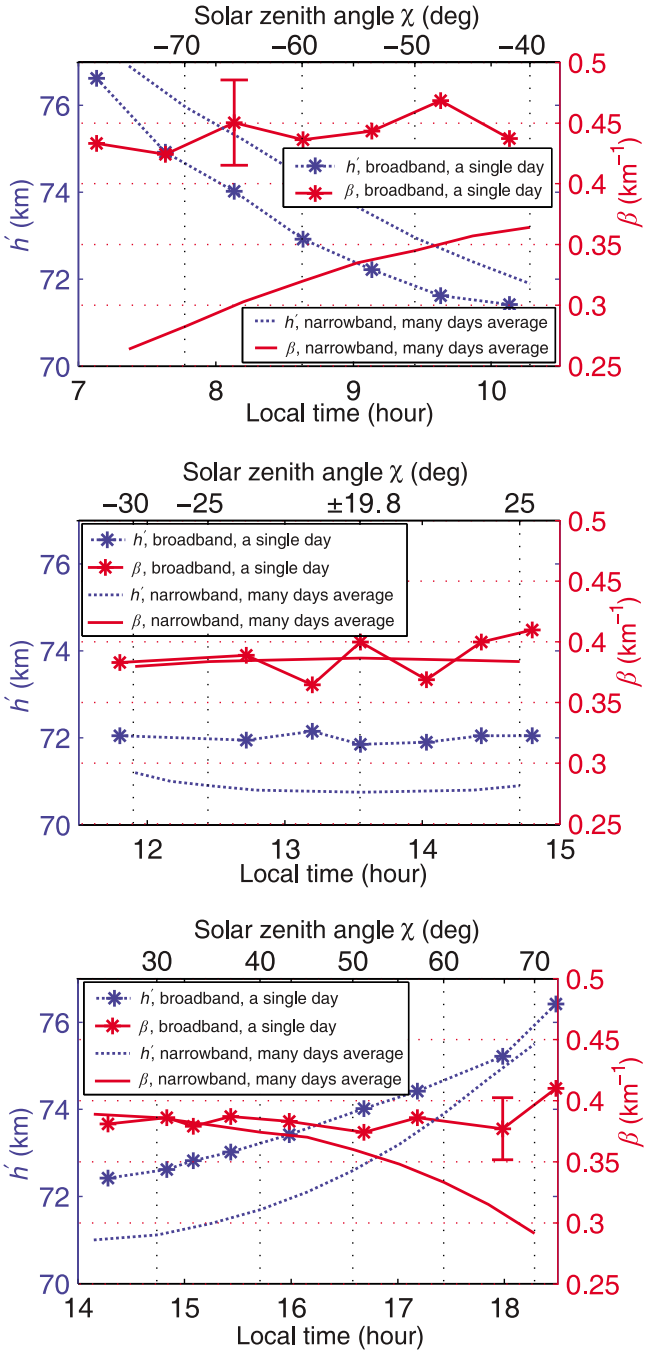

Figure 3. Measured h' and β from broadband sferics compared to narrowband measurements from *McRae and Thomson* [2000]. (top) Broadband measurements on 19 July 2005 compared to narrowband measurements from several-day averages during the morning period, (middle) broadband measurements on 12 August 2005 compared to narrowband measurements from several-day averages during the noontime period, and (bottom) broadband measurements on 6 August 2005 compared to narrowband measurements from several-day averages during the afternoon period.

surement error caused by the waveguide mode interference pattern alignment uncertainty is ±0.023 km^{-1}.

[19] We applied the β derivation procedure to 23 cases of 5 min averaged sferic spectra to infer the β for solar zenith angles between 20° and 75° (the minimum observable value given our sensor latitude) for morning, noon, and afternoon measurements. Figure 3 (top) shows the measured h' and β variations with local time and solar zenith angles from broadband sferics and narrowband VLF signals [*McRae and Thomson*, 2000] during the morning period. We only discuss the broadband measurements in section 4 and will discuss their comparisons with narrowband measurements in section 5. The broadband sferics were excited by lightning strokes in the east coast of United States and 720–760 km from Duke sensors in the morning on 19 July 2005. Since more than half of sferic wave propagation paths were over the ocean, we used PEC as the ground boundary condition in FDTD simulations for this group of sferics. We computed seven h' and β values across a 3.5 h time window, i.e., one measurement in around every 30 min. The h' decreased with decreasing solar zenith angle, which is consistent with all previous measurements [*McRae and Thomson*, 2000; *Han and Cummer*, 2010b]. In order to distinguish the period before and after noontime, we label the morning solar zenith angle as negative values [*McRae and Thomson*, 2000]. The measured β was around 0.45 km^{-1} with some uncertainties during the 3.5 h period. By computing other two cases when the solar zenith angle was between 60° and 70° in the morning, we estimated the β day-to-day variation ±0.035 km^{-1}, which is shown by the error bar in Figure 3 (top). Given this uncertainty, the measured β is consistent with a completely uniform value, and the measured average value is β = 0.44 km^{-1}. The slight increase in morning β with time is probably not significant.

[20] As shown in Figure 3 (middle), during the noontime period, both the measured h' and β were different from in the morning. NLDN recorded lightning strokes from the west of Duke sensors and 660–720 km away on 12 August 2005 were used to measure the average electron densities across the sferic wave propagation paths. We used the SIBC ground boundary since sferic wave propagation paths were over land. In this 3 h period, as expected [*McRae and Thomson*, 2000; *Han and Cummer*, 2010b], the h' was relatively stable. The measured β was again essentially constant with solar zenith angle, given the measurement uncertainties, with an average value of β = 0.39 km^{-1}.

[21] Figure 3 (bottom) shows h' and β variations during the afternoon period on 6 August 2005. The lightning strokes used in these measurements were located in the northeast (azimuth angle ~60°) of and 720–800 km from the Duke sensors. The ground boundary was treated as a PEC because most wave propagation paths were primarily over the ocean. The h' increased as the solar zenith angle increased, as expected. However, once again, the measured β during this 4 h period was essentially constant with an average value of β = 0.38 km^{-1}. We also estimated the day-to-day variation ±0.026 km^{-1} using the similar method as for the morning period.

[22] These measurements in three daytime periods showed that our measured daytime β, while it may exhibit modest day-to-day variability, has only a weak dependence on solar zenith angle from morning, through noontime, and into the

afternoon. This is in sharp contrast to the measured h' [*Han and Cummer*, 2010b] which does exhibit a very clear solar zenith angle dependence. Below we compare these measurements to previously reported measurements of the same quantities and also these quantities extracted from modeled daytime ionosphere electron density profiles.

5. Comparisons With Other Measured or Modeled Results

[23] In our work, β was measured from the mode interference pattern in the higher-frequency range of broadband VLF sferic spectra. Several other measurements have also been presented in previous work. *McRae and Thomson* [2000] calculated the β dependence on solar zenith angles from amplitudes and phases of narrowband VLF signals over a variety of long subionospheric paths. There are significant differences between the measurement approaches in our work and this previous work, i.e., narrowband versus broadband VLF, short versus long propagation paths, but a comparison is still valuable. We also analyzed the effective h' and β obtained from IRI and FIRI modeled daytime electron density profiles.

5.1. Comparison With Narrowband VLF Measurements

[24] Following the work by *Thomson* [1993], *McRae and Thomson* [2000] calculated curves for the dependence of h' and β on solar zenith angles by comparing LWPC modeled VLF amplitudes and phases with diurnal observed results in a few days over several long and short paths. In the next step, they verified their measurements by comparing the observed and model calculated amplitude and phase variations with time of the day using LWPC and based on their measured h' and β for four different VLF transmitters including Omega Hawaii, Omega Japan, NPM Hawaii and NLK Seattle. The comparisons between their measurements and our measurements are shown in Figure 3. During the morning period, as shown in Figure 3 (top), β from narrowband measurements showed obvious monotonic ascending trend, increasing from 0.26 km^{-1} when the solar zenith angle χ was 75° to 0.36 km^{-1} for χ = 40°. However, these absolute values were significantly smaller compared to our broadband measurements. They were about 0.15 km^{-1} smaller than our broadband measurements in the early morning, and this difference decreased to around 0.05 km^{-1} at 1008 LT.

[25] In contrast, the absolute values of β calculated by *McRae and Thomson* [2000] are in close agreement with our broadband measurements during the noontime period, which is shown in Figure 3 (middle). During the afternoon period, as shown in Figure 3 (bottom), narrowband measured β showed obvious descending trend. It was consistent with broadband measured β when the solar zenith angle was smaller. But it kept decreasing as the solar zenith angle increasing while β from broadband measurements did not change obviously during the same period.

[26] In the narrowband measurements given by *McRae and Thomson* [2000], the parameter β was inversely correlated to the solar zenith angle. In our broadband measurements, β did not show any obvious increasing and decreasing trends during morning and afternoon periods. Narrowband measured β variation was almost symmetrical for the morning and afternoon; that is, the β value was almost the same for the same solar zenith angle during morning and afternoon periods. In broadband measurements, β during the morning period was ~0.05 km^{-1} larger than it in the afternoon period. However, this difference may be attributable to simple daily variability given the small number of measurements in the broadband data set.

[27] It should again be emphasized that the measurement techniques compared here are different, particularly because of the disparate propagation lengths. Our broadband measurement employs short propagation paths and is thus highly local compared to the long-path narrowband technique. Nevertheless it is somewhat surprising that these techniques exhibit such a significant discrepancy in the measured daytime β given that they agree quite closely in the measured nighttime and daytime h' [*Han and Cummer*, 2010a, 2010b].

5.2. Comparison With IRI Model

[28] The IRI is a widely used standard for the specification of ionosphere parameters and is recommended for international use [*Bilitza*, 2001]. For a given time and location, it provides an empirical standard model of the ionospheric electron density and other parameters in the altitude range from ~60 km to ~2000 km based on all kinds of data source. Here we treat propagation simulations with IRI ionospheres as synthetic data and extract the effective h' and β to gain some insight into the relationship of these parameters to more complex ionospheric electron density profiles.

[29] We fitted several simulated sferic spectra from using two-parameter exponential electron density profiles to the simulated sferic spectrum from using a certain IRI model, and calculated the best fitted h' and β. In all the FDTD simulations, we set the azimuth angle as 90° and the distance as 700 km. And only the PEC ground boundary condition was used. Figures 4a and 4b show an example for the sferic spectrum fitting between that from using IRI-2001 model and that from using the exponential profile. The good fitting in both the lower- and higher-frequency range means that the best fitted parameters for the IRI-2001 profile are h' = 72.0 km and β = 0.35 km^{-1}. Figure 4c shows the comparison between the IRI-2001 modeled electron density profile and the best fitted exponential profile. The two profiles are rather consistent in the electron density range ~40–400 cm^{-3}, indicating that it is the electron densities in this range that contribute most strongly to VLF propagation characteristics. The electron density below 60 km is not given in the IRI model. We extended the electron density to lower altitudes according to the profile variation trend above 60 km. However, because the electron density below 60 km is rather small, the simulated sferic feature does not change even if the density below 60 km is increased two times.

[30] By applying this fitting procedure, we derived the best fitted h' and β for both IRI-2001 and IRI-2007 *D* region electron density profiles during the morning period on 19 July 2005 near Duke University. In 3 h from 07 LT to 10 LT, we calculated seven sets of best fitted h' and β with each set in every half hour. Compared to the broadband measured results during the same time, which are shown in Figure 3 (top), the h' derived from both IRI-2001 and IRI-2007 are lower before 0830 LT but higher after that time. It means h' decreasing during the morning period is slower from the IRI

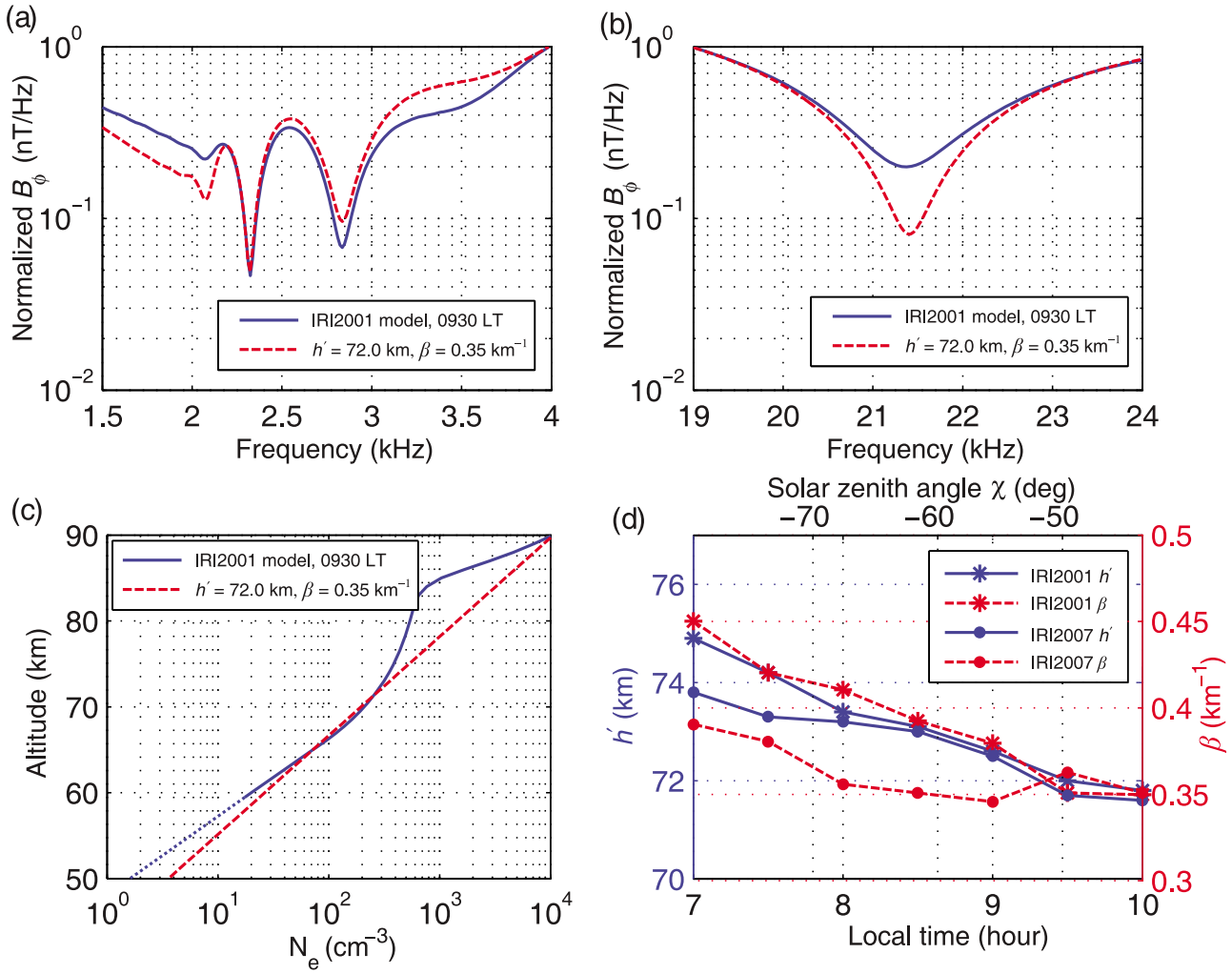

Figure 4. The equivalent h' and β for IRI during the morning period on 19 July 2005: (a) h' derived from the lower-frequency mode interference pattern, (b) β derived from the higher-frequency mode interference pattern, (c) the best fitted exponential profile compared to IRI-2001 modeled profile at 0930 LT (electron density in the IRI model below 60 km is extended from its variation trend above 60 km and plotted as dotted line), and (d) the best fitted h' and β in 3 h during the morning period.

model than for the practical measured results using broadband sferics. In addition, there are also difference for the h' for IRI-2001 and IRI-2007. From07 LT to 08 LT, the derived h' difference between IRI-2001 and IRI-2007 model decreased from 1.1 km to 0.2 km.

[31] While the extracted h' measurements are in good agreement with our broadband and past narrowband measurements, the derived β values from the IRI model are significantly different from both measurements. In IRI-2001 model, the derived β decreases monotonically from 0.45 km^{-1} at 07 LT to 0.35 km^{-1} at 10 LT. In IRI-2007 model, the derived β decreases from 0.39 km^{-1} at 07 LT to near 0.35 km^{-1} at 09 LT. And then, it increases to 0.36 km^{-1} at 0930 LT. The absolute values of β from IRI-2001 and IRI-2007 are smaller than those from our broadband measurements. In addition, the β variation trends from the IRI model are opposite to the results given by *McRae and Thomson* [2000] since β increases during the morning period in their measurements. The β values from the IRI model are in closer quantitative agreement with our broadband measurements compared to narrowband measurements, although the IRI model exhibits a consistent trend not seen in the broadband measurements.

5.3. Comparison With FIRI Model

[32] The FIRI is a semiempirical lower ionosphere model which is exclusively based on Faraday rotation experiments [*Friedrich and Torkar*, 2001]. We adapted three typical daytime electron density profiles for solar zenith angles 30°, 60° and 75° from the FIRI model given by *Friedrich and Torkar* [2001]. In the original work, no electron density below 60 km was provided. We use the similar method as for the IRI model to construct the electron density below this altitude. These profiles are for the condition of low latitude, January and low solar activity. Figures 5a and 5b show the best fitted h' = 71.8 km and β = 0.28 km^{-1} derived from sferic spectrum fitting, which is similar to the method we used for IRI model.

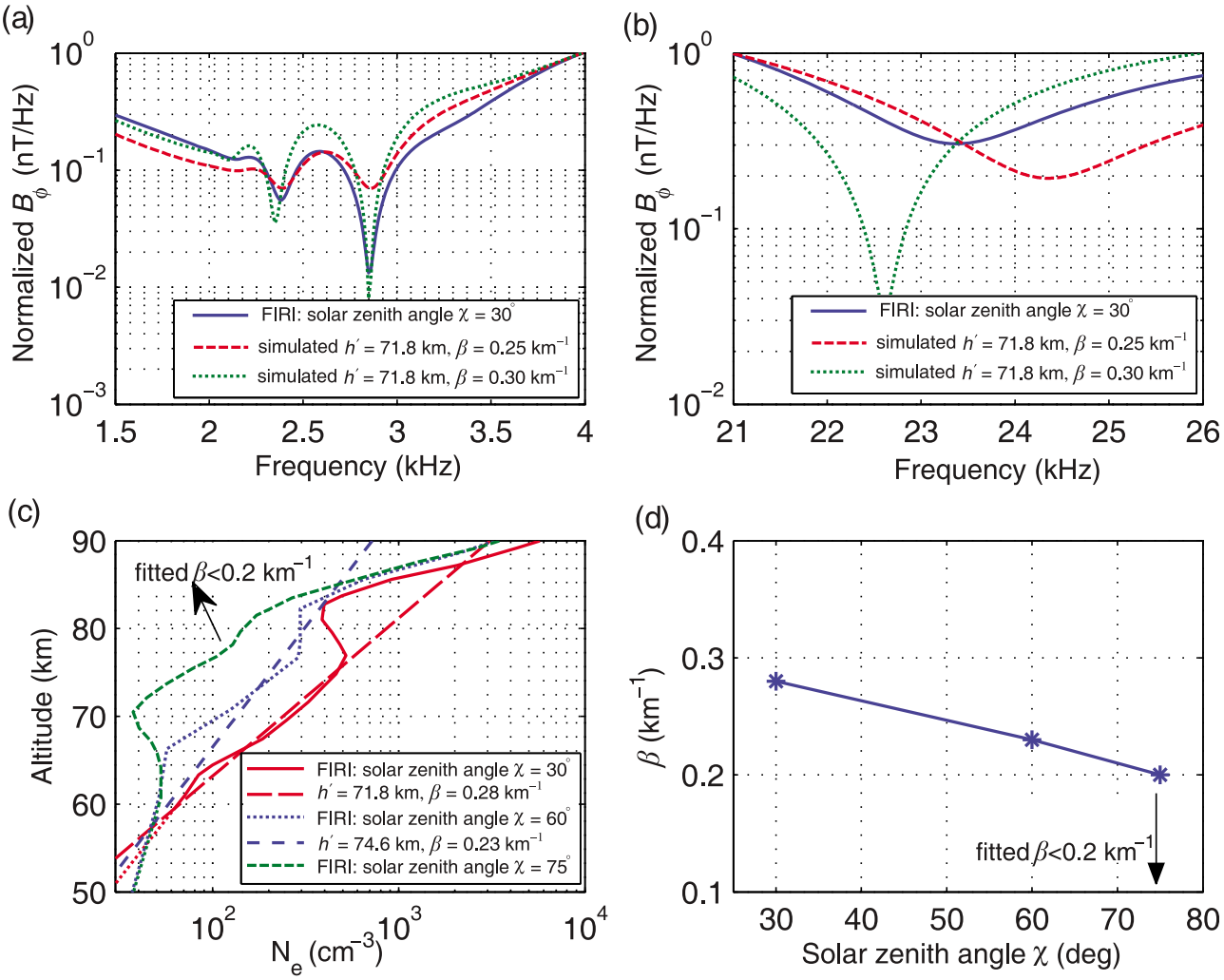

Figure 5. The electron density profiles from FIRI [*Friedrich and Torkar*, 2001] fitted by exponential profiles (below 60 km altitude, the FIRI profiles are extended from their variation trends above 60 km and are plotted as dotted lines): (a) h' derived from the lower-frequency mode interference pattern for solar zenith angle $\chi = 30°$; (b) β derived from the higher-frequency mode interference pattern for solar zenith angle $\chi = 30°$; (c) the best fitted profiles were found for solar zenith angles 30° and 60°, and the best fitted β for $\chi = 75°$ is smaller than 0.2 km^{-1} and near 0.15 km^{-1}, which is meaningless in physics; and (d) the best fitted β changes with solar zenith angle variations.

[33] Figure 5c shows the comparison between electron density profiles from FIRI and the best fitted exponential profiles. For the solar zenith angle 30°, the best fitted h' is 71.8 km and the best fitted β is 0.28 km^{-1}. The h' value is near our measured value from broadband sferics and that provided by *McRae and Thomson* [2000] for the same solar zenith angle. However, the best fitted $\beta = 0.28$ km^{-1} is much smaller than our measured value 0.39 km^{-1} when the solar zenith angle was 30° during the afternoon period on 6 August 2005. It is also smaller than the measured value 0.39 km^{-1} given by *McRae and Thomson* [2000]. When the solar zenith angle is 60°, the measured β decreased to 0.23 km^{-1}. This value is also smaller than both broadband and narrowband measured values. When the solar zenith angle increases to 75°, there is no existing equivalent exponential profile since the derived β is less then 0.2 km^{-1} and near 0.15 km^{-1}. It becomes meaningless in physics since the electron density in the exponential profile is a constant when $\beta = 0.15$ km^{-1}. And the β variation trend with solar zenith angle increasing is shown in Figure 5d. It is consistent with the result given by *McRae and Thomson* [2000]. However, the absolute values of β for FIRI are ~0.1 km^{-1} smaller than those from *McRae and Thomson* [2000].

6. Summary and Conclusions

[34] In this work, we derived the midlatitude *D* region equivalent exponential electron density profile sharpness by comparing the higher-frequency mode interference pattern of measured sferic spectra to FDTD model simulated results. The β values during morning, noontime and after-

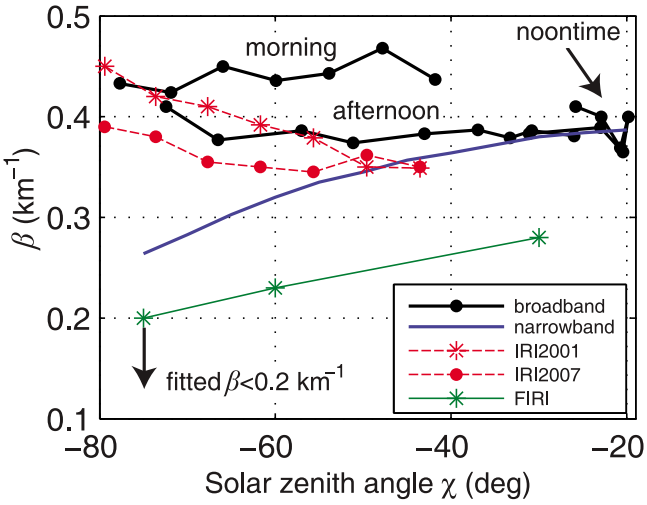

Figure 6. The summary of β value changes with solar zenith angles, assuming all measurements in the morning period. Broadband measurements in three different periods are labeled. All the β measurements are different. Broadband measured β is independent of the solar zenith angle and close to the values extracted from IRI models. The β values from the FIRI model are the lowest. The β values from all kinds of measurements and models are more consistent when the solar zenith angleis small than when it is large.

noon periods in 3 different days were extracted from broadband VLF propagation spectra obtained on relatively short (~700 km) propagation paths. This β measured from broadband VLF sferic spectra was compared to narrowband VLF measurements, IRI model and FIRI model. The comparisons of all these measurements, assumed in the morning period, are shown in Figure 6.

[35] The estimated β from all these sources are surprisingly different. Our broadband, short-path measurements show a β that is relatively independent of solar zenith angle with a value around 0.39 km^{-1} (although this value may be somewhat variable from day to day). This value is close to the average value extracted from the IRI model ionospheres, but the IRI ionospheres also show a clearly decreasing β as time moves toward noon. The narrowband, long-path measurements given by *McRae and Thomson* [2000] show lower values of β from about 0.25 to 0.38 km^{-1} with a clearly increasing β as time moves toward noon (the opposite trend from the IRI ionospheres). The FIRI model ionospheres exhibit the lowest β values of all, varying from about 0.20 to 0.30 km^{-1} also with a clearly increasing β as time moves toward noon.

[36] For solar zenith angles less than about 45°, the broadband measurements, the narrowband measurements, and the IRI model values are all in reasonably close agreement, exhibiting β = 0.35 to 0.40 km^{-1} that is weakly or not dependent on solar zenith angle. The FIRI values are lower and more dependent on solar zenith angle. But for higher solar zenith angles, these different sources exhibit strong differences in the values of β that they predict. This suggests that the daytime ionosphere electron density profiles for times significantly away from local noon (i.e., higher solar zenith angles) may not be well approximated by a simple two-parameter exponential profile.

[37] **Acknowledgments.** This research was supported by an NSF Aeronomy Program grant. The IRI-2001 data were downloaded from http://modelweb.gsfc.nasa.gov/models/iri.html. The IRI-2007 data were downloaded from http://omniweb.gsfc.nasa.gov/vitmo/iri_vitmo.html.

[38] Philippa Browning thanks the reviewers for their assistance in evaluating this paper.

References

Balanis, C. A. (1989), *Advanced Engineering Electromagnetics*, chap. 4, p. 62, John Wiley, Dordrecht, Netherlands.

Bilitza, D. (2001), International Reference Ionosphere 2000, *Radio Sci.*, *36*, 261–275.

Cheng, Z., and S. A. Cummer (2005), Broadband VLF measurements of lightning-induced ionospheric perturbations, *Geophys. Res. Lett.*, *32*, L08804, doi:10.1029/2004GL022187.

Cheng, Z., S. A. Cummer, D. N. Baker, and S. G. Kanekal (2006), Nighttime D region electron density profiles and variabilities inferred from broadband measurements using VLF radio emissions from lightning, *J. Geophys. Res.*, *111*, A05302, doi:10.1029/2005JA011308.

Cummer, S. A., U. S. Inan, and T. F. Bell (1998), Ionospheric D region remote sensing using VLF radio atmospherics, *Radio Sci.*, *33*, 1781–1792.

Cummins, K. L., E. P. Krider, and M. D. Malone (1998), The U.S. national lightning detection network and applications of cloud-to-ground lightning data by electric power utilities, *IEEE Trans. Electromagn. Compat.*, *40*, 465–480.

Dennis, A. S., and E. T. Pierce (1967), The return stroke of the lightning flash to Earth as a source of VLF atmospherics, *Radio Sci.*, *68*, 772–794.

Fine, H. (1954), An effective ground conductivity map for continental United States, *Proc. IRE*, *42*(9), 1405–1408.

Friedrich, M., and K. M. Torkar (1983), Collision frequencies in the high-latitude D-region, *J. Atmos. Terr. Phys.*, *45*, 267–271.

Friedrich, M., and K. M. Torkar (2001), FIRI: A semiempirical model of the lower ionosphere, *J. Geophys. Res.*, *106*(A10), 21,409–21,418.

Han, F., and S. A. Cummer (2010a), Midlatitude nighttime D region ionosphere variability on hourly to monthly timescales, *J. Geophys. Res.*, *115*, A09323, doi:10.1029/2010JA015437.

Han, F., and S. A. Cummer (2010b), Midlatitude daytime D region ionosphere variations measured from radio atmospherics, *J. Geophys. Res.*, *115*, A10314, doi:10.1029/2010JA015715.

Hu, W., and S. A. Cummer (2006), An FDTD model for low and high altitude lightning-generated EM fields, *IEEE Trans. Antennas Propag.*, *54*, 1513–1522.

Jacobson, A. R., R. Holzworth, E. Lay, M. Heavner, and D. A. Smith (2007), Low-frequency ionospheric sounding with narrow bipolar event lightning radio emissions: Regular variabilities and solar X-ray responses, *Ann. Geophys.*, *25*, 2175–2184.

Jacobson, A. R., X.-M. Shao, and R. Holzworth (2009), Full-wave reflection of lightning long-wave radio pulses from the ionospheric D region: Numerical model, *J. Geophys. Res.*, *114*, A03303, doi:10.1029/2008JA013642.

Jacobson, A. R., X.-M. Shao, and R. Holzworth (2010), Full-wave reflection of lightning long-wave radio pulses from the ionospheric D region: Comparison with midday observations of broadband lightning signals, *J. Geophys. Res.*, *115*, A00E27, doi:10.1029/2009JA014540.

Jones, D. L. (1970), Electromagnetic radiation from multiple return strokes of lightning, *J. Atmos. Terr. Phys.*, *32*, 1077–1093.

Kellali, S., and B. Jecko (1993), Implementation of a surface impedance formalism at oblique incidence in FDTD method, *IEEE Trans. Electromagn. Compat.*, *35*, 347–356.

Li, J., S. A. Cummer, W. A. Lyons, and T. E. Nelson (2008), Coordinated analysis of delayed sprites with high-speed images and remote electromagnetic fields, *J. Geophys. Res.*, *113*, D20206, doi:10.1029/2008JD010008.

Maloney, J. G. (1992), The use of the surface impedance concepts in the finite-difference time-domain method, *IEEE Trans. Antennas Propag.*, *40*, 38–48.

McRae, W. M., and N. R. Thomson (2000), VLF phase and amplitude: Daytime ionospheric parameters, *J. Atmos. Sol. Terr. Phys.*, *62*, 609–618.

McRae, W. M., and N. R. Thomson (2004), Solar flare induced ionospheric D-region enhancements from VLF phase and amplitude observations, *J. Atmos. Sol. Terr. Phys.*, *66*, 77–87.

Morfitt, D. G., and C. H. Shellman (1976), MODESRCH: An improved computer program for obtaining ELF/VLF/LF mode constants in an

Earth–ionosphere waveguide, Nav. Electron Lab. Cent., San Diego, Calif.

Narcisi, R. S. (1971), Composition studies of the lower ionosphere, in *Physics of the Upper Atmosphere*, edited by F. Verniani, pp. 21–56, Compositori, Bologna, Italy.

Pappert, R. A., and J. A. Ferguson (1986), VLF/LF mode conversion model calculations for air to air transmissions in the Earth-ionosphere waveguide, *Radio Sci.*, *21*, 551–558.

Phelps, A. V., and J. L. Pack (1959), Electron collision frequencies in nitrogen and in the lower ionosphere, *Phys. Rev. Lett.*, *3*, 340–342.

Smith, D. A., M. J. Heavner, A. R. Jacobson, X. M. Shao, R. S. Massey, R. J. Sheldon, and K. C. Wiens (2004), A method for determining intracloud lightning and ionospheric heights from VLF/LF electric field records, *Radio Sci.*, *39*, RS1010, doi:10.1029/2002RS002790.

Thomson, N. R. (1993), Experimental daytime VLF ionospheric parameters, *J. Atmos. Terr. Phys.*, *55*, 173–184.

Thomson, N. R. (2010), Daytime tropical D region parameters from short path VLF phase and amplitude, *J. Geophys. Res.*, *115*, A09313, doi:10.1029/2010JA015355.

Thomson, N. R., and M. A. Clilverd (2001), Solar flare induced ionospheric D-region enhancements from VLF amplitude observations, *J. Atmos. Sol. Terr. Phys.*, *63*, 1729–1737.

Thomson, N. R., and W. M. McRae (2009), Nighttime ionospheric region: Equatorial and nonequatorial, *J. Geophys. Res.*, *114*, A08305, doi:10.1029/2008JA014001.

Thomson, N. R., C. J. Rodger, and R. L. Dowden (2004), Ionosphere gives size of greatest solar flare, *Geophys. Res. Lett.*, *31*, L06803, doi:10.1029/2003GL019345.

Thomson, N. R., C. J. Rodger, and M. A. Clilverd (2005), Large solar flares and their ionospheric D region enhancements, *J. Geophys. Res.*, *110*, A06306, doi:10.1029/2005JA011008.

Thomson, N. R., M. A. Clilverd, and W. M. McRae (2007), Nighttime D region parameters from VLF amplitude and phase, *J. Geophys. Res.*, *112*, A07304, doi:10.1029/2007JA012271.

Thrane, E. V., and W. R. Piggott (1966), The collision frequency in the E- and D-regions of the ionosphere, *J. Atmos. Terr. Phys.*, *28*, 721–737.

Wait, J. R., and K. P. Spies (1964), *Characteristics of Earth-Ionosphere Waveguide for VLF Radio Waves*, Natl. Bur. of Stand., Boulder, Colo.

S. A. Cummer, F. Han, J. Li, and G. Lu, Department of Electrical and Computer Engineering, Duke University, Durham, NC 27708, USA. (cummer@ee.duke.edu; feng.han@duke.edu; jl108@ee.duke.edu; gl46@duke.edu)